Cellular and Molecular Life Sciences (2025) 82:208
https://doi.org/10.1007/s00018-025-05721-w

ORIGINAL ARTICLE

Inflammatory metabolite 7α,25-OHC promotes TIMP1 expression in COVID-19 monocytes through synergy effect of SMARCC1/JUND/H3K27ac

Ying Feng[1] · Zheng Wu[1] · Kefan Hu[2] · Shenzhen Yuan[1] · Jun Li[1] · Yi Wang[1] · Zhongyi Wang[1] · Han Yang[1] · Zhi-Hui Luo[1] · Jingjiao Zhou[1]

Received: 8 December 2024 / Revised: 24 March 2025 / Accepted: 19 April 2025

Abstract

Chromatin remodeling factors are involved in the inflammatory responses, contributing to tissue damage and multi-organ dysfunction in COVID-19 patients. However, the underlying mechanisms remain unclear. In this study, high-dimensional analyses of single-cell RNA sequencing and single-cell ATAC sequencing data revealed increased chromatin accessibility at the promoters or enhancers of the pro-inflammatory cytokine tissue inhibitor of metalloproteinase-1 (TIMP1), as well as altered gene transcription profiles in monocytes from COVID-19 patients. Motif enrichment and positive regulators analyses identified SMARCC1, the core subunit of the chromatin remodeling complex, and the transcription factor JUND as positive regulators to co-modulate TIMP1 expression. In-vitro experiments, co-immunoprecipitation and chromatin immunoprecipitation (ChIP)-qPCR, and others, demonstrated the collaboration of SMARCC1 and JUND. Increased 7α,25-dihydroxycholesterol (7α,25-OHC) enhanced SMARCC1-JUND interactions to co-regulate TIMP1 expression. Further investigation indicated that 7α,25-OHC promoted the expression of SMARCC1 and its co-localization with H3K27ac, which involved in the expression of TIMP1 and inflammatory responses. Our study highlights the critical roles of SMARCC1 and JUND in COVID-19 inflammation, and offers the potential targets for the prevention and treatment of COVID-19.

Keywords COVID-19 · Monocyte · SMARCC1 · TIMP1 · Chromatin remodeling

Introduction

Coronavirus disease 2019 (Abbreviated as COVID-19), caused by the SARS-CoV-2 coronavirus, resulting in hundreds of millions of infections and millions of deaths worldwide. Research indicated that 10–20% of SARS-CoV-2-infected individuals experience persistent symptoms lasting for several months or even years [1]. Symptoms that remain for at least three months after SARS-CoV-2 infection are classified as Long COVID. Patients who experience severe illness are at higher risk of developing Long COVID [2]. Widespread vaccination significantly decreases the incidence of severe COVID-19 and mortality, however, reinfections become increasingly common due to the emergence of new SARS-CoV-2 variants [3]. The increased duration of infection, along with multiple reinfections, further elevates the likelihood of Long COVID [1]. Consequently, it remains practical significance to delve into the underlying pathogenic mechanisms of COVID-19.

Ying Feng, Zheng Wu and Kefan Hu contributed equally to this work.

Jingjiao Zhou is lead contact.

✉ Han Yang
yanghan@wust.edu.cn

✉ Zhi-Hui Luo
luozhihui@wust.edu.cn

✉ Jingjiao Zhou
zhoujj@wust.edu.cn

[1] Department of Biology and Genetics, The College of Life Sciences and Health, Wuhan University of Science and Technology, Wuhan, Hubei, China

[2] Department of Biology, Faculty of Science, Hong Kong Baptist University, Hong Kong, SAR, China

Published online: 21 May 2025

Cytokines are key regulators of the immune response, and their excessive release can lead to uncontrolled inflammation, and multi-organ disfunction in various diseases [4]. For instance, elevated levels of tissue inhibitor of metalloproteinase-1 (TIMP1) have been linked to the progression of multiple inflammatory diseases including pancreatic cancer, sepsis and inflammatory malignancies [5]. Excessive IL-18 led to lung injury in influenza and SARS, as well as subsequently potential cardiac inflammation and fibrosis [6]. SARS-CoV-2 infection can trigger dysregulation of the host immune response, leading to overabundance of pro-inflammatory cytokines, CCL2, IL-1, IL-6, and CCL8, etc. [7]. Up to 12 months after SARS-CoV-2 infection, some COVID-19 patients still experienced persistent inflammation and activation of immune cells [8]. Despite the use of tocilizumab (an IL-6 inhibitor) and anakinra (an IL-1 receptor blocker) showing effectiveness, only a minority of COVID-19 patients benefit from these treatments [9]. Thus, it is necessary to further investigate the new inflammatory factors and their underlying production mechanisms in COVID-19.

Monocytes/macrophages contribute to the initiation of inflammatory responses and exacerbate disease progression by producing and releasing pro-inflammatory cytokines, including IL-6, IL-1β, IL-18, and IFN-α, etc. [10, 11]. Ly6C high-expressing monocytes can trigger inflammatory responses, accelerating liver fibrosis and hepatic pathological progression in myocardial infarction [12]. Additionally, in the autoimmune disease VEXAS (vacuoles, E1 enzyme, X-linked, autoinflammatory, somatic) syndrome, monocytes exhibit signs of hyperactivation, with high expression of inflammatory factors such as IL-1β and IL-18, which further amplifies the inflammatory response and exerts a detrimental effect on disease progression [13]. Monocytes also play a critical role in the immune response in SARS-CoV-2 infection [14, 15].

The expression patterns of inflammatory cytokines are regulated at multiple levels, including gene transcriptional, post-transcriptional, translational, and post-translational level. At transcriptional level, gene transcriptional activity is controlled by cell-specific chromatin structures. Cis-regulatory elements such as promoters and enhancers, ATP-dependent chromatin remodeling complexes and transcription factors (TFs) play essential roles in gene transcription [16]. Recent studies have demonstrated that SARS-CoV-2 infection can disrupt the host cell epigenetic regulation, affecting chromatin structure within the cell nucleus and altering immune genes expression [17, 18]. However, the characteristics of chromatin accessibility, cis-regulatory elements, and the trans-acting factors driving epigenetic changes in monocytes following SARS-CoV-2 infection remain poorly understood. A comprehensive mechanistic investigation is necessary to elucidate the epigenetic regulation of pro-inflammatory cytokines in monocytes.

In this study, we analyzed single-cell assay for transposase-accessible chromatin using sequencing (scATAC-seq) data and single-cell RNA sequencing (scRNA-seq) data of peripheral blood mononuclear cells (PBMCs) from COVID-19 patients. The results revealed the epigenetic regulatory features of transcriptional processes in monocytes and identified key cis-regulatory elements and trans-acting factors involved in the transcription of pro-inflammatory cytokines, TIMP1, CX3CR1 and CCR1, etc. In-vitro experiments, chromatin immunoprecipitation (ChIP)-qPCR and co-immunoprecipitation (Co-IP), etc., confirmed that the core subunit of the chromatin remodeling complexes, SMARCC1, and TF JUND collaboratively regulated the expression of pro-inflammatory cytokine, including TIMP1. Further examinations indicated that hydroxy sterol 7α,25-dihydroxycholesterol (7α,25-OHC), increased the expression of SMARCC1 and JUND, and histone acetylation of H3 lysine 27 (H3K27ac), which may participate in the expression of pro-inflammatory cytokine TIMP1, etc. This study provides new insights into the regulatory mechanisms of monocyte inflammation and simultaneously establishes a robust theoretical foundation for strategies to prevent and treat COVID-19.

Materials and methods

Cell lines, drugs and antibodies

THP-1 cells (ATCC, USA) were cultured in RPMI-1640 medium containing 10% FBS, 1% penicillin–streptomycin, and 1 × β-mercaptoethanol. These cells were incubated in 5% CO_2 incubator at 37 °C and used for various experiments. The metabolite 7α,25-OHC was purchased from Cayman (USA) and the antagonist NIBR189 was purchased from TargetMol (USA). THP-1 cells were stimulated with 100 nM or 1 μM 7α,25-OHC and/or 1 μM NIBR189 respectively for 18 h. Antibodies used in the study include JUND antibody (ABclonal, CHN), SMARCC1 antibody (Proteintech, CHN), Tubulin antibody (Proteintech, CHN), H3K27ac antibody (PTM BIO, CHN) and β-Actin antibody (ABclonal, CHN).

Quality control, dimensionality reduction and clustering for scATAC-seq and scRNA-seq datasets

scRNA-seq and scATAC-seq datasets (5 healthy individuals and 10 COVID-19 patients) of human PBMCs were accessed from the GEO database (GSE206283 and GSE206455 datasets) [19].

Using ArchR (v1.0.2) and Seruat (v4.3.0) to analyzed scATAC-seq and scRNA-seq datasets, respectively [20, 21].

For scATAC-seq, low-quality cells were excluded by applying criteria including unique fragment count (> 1,000) and transcription start site (TSS) enrichment (> 4), with doublets also removed. Low-quality cells were excluded by applying criteria as mitochondrial reads > 10%, expressed genes < 200 or > 4000, and genes expressed in fewer than three cells were removed from subsequent analysis for scRNA-seq,

For scATAC-seq, a low-dimensional matrix of these cells was generated using scOpen (v1.0.0) [22]. Clusters were annotated by generating a GeneScoreMatrix using the 'addGeneScoreMatrix' function and 'getMarkerFeatures' function. After performing quality control on the scRNA-seq data, we used the 'vst' method in Seurat to determine principal component analysis using the top 2,000 most variable features. Then, cells were clustered using the first 15 principal components. Visualization of the scATAC-seq and scRNA-seq cell clusters were achieved using the Uniform Manifold Approximation and Projection (UMAP). Cells were annotated based on gene expression levels or gene activity scores of marker gene for each cluster [23].

Peak calling and marker peak detection in scATAC-seq data

For peak calling, we used the Macs2 algorithm to generate reproducible peak matrix for comparing differential open chromatin accessibility. The differentially accessible peaks (DAPs) were identified for each cell type and disease condition, and peaks with an FDR < 0.1 and $|Log_2FC| > 0.5$ were considered DAPs.

Sub-clustering of monocyte compartments

In scATAC-seq and scRNA-seq datasets, the monocytes were extracted and investigated for further analyses, respectively. For scATAC-seq, we used the top-30 dimensions and top-25,000 variable features to perform iterative latent semantic indexing. Next, we clustered cells using the IterativeLSI reduced dimensions with a resolution of 0.8, followed by UMAP computation with parameters set to nNeighbors = 30 and minDist = 0.5. For scRNA-seq, the cells were clustered based on the top-30 principal components with a resolution of 0.3. We applied UMAP based on the top-30 principal components for visualization.

Differentially accessible peaks/expressed genes and functional enrichment analyses

For comparison between healthy and COVID-19 conditions, DAPs were performed using the 'getMarkerFeatures' function in ArchR, and differentially expressed genes (DEGs) were performed using the 'FindMarkers' function in Seurat. Peaks with FDR < 0.1 and $|Log_2FC| > 0.5$ were regarded as significantly DAPs. Genes with p-value < 0.05 were regarded as significantly DEGs.

To perform peak clustering and annotate peaks with the nearest genes for monocyte, the 'addGroupCoverages' and 'addReproduciblePeakSet' functions were used. Using ClusterProfiler (v4.2.2) to analyze the functional enrichment of DAPs -related genes, including Gene Ontology (GO) terms and Kyoto Encyclopedia of Genes and Genomes (KEGG) pathways.

Combined analysis of scATAC-seq dataset with scRNA-seq dataset

To integrate analyze the scATAC-seq and scRNA-seq datasets, we compared the scATAC-seq cell-independent gene score matrix with the scRNA-seq gene expression matrix. This integration aligned all cells from scATAC-seq with those from scRNA-seq. Subsequently, we aligned the scATAC-seq cells with the cells in the scRNA-seq clusters and added gene integration scores to each cell, creating a gene-integration matrix.

To identify potential regulatory relationships from peaks to genes, we used the 'addPeak2GeneLinks' function to calculate the correlation between peak accessibility from scATAC-seq and gene expression from scRNA-seq. Links with co-accessibility > 0.2 and FDR < 0.05 were regarded as regulatory links.

Transcription factor motif annotation and enrichment

After peak calling, we sought to identify enriched motifs within openly accessible peak of monocytes under various conditions. We first applied CIS-BP database to add motif annotations using the 'addMotifAnnotations' function. We then identified motifs that were overrepresented in the peak sets using the 'peakAnnoEnrichment' function in ArchR. We used the 'ggplot' function to visualize the enriched motifs. For peak annotation, we utilized the 'addDeviationsMatrix' function from HOMER. Additionally, we calculated ChromVAR bias scores for these motifs using ArchR. Positively regulated TFs were defined as whose inferred gene scores are correlated to their chromVAR TF deviation z-scores. TFs with the maximum disparities in chromVAR deviation z-scores within the top quartile, adjusted p-value below 0.01 and correlation coefficient exceeding 0.3 were considered positive regulators. Visualization of TF motifs using the seqLogo package.

Chromatin accessibility of COVID-19 eQTL

We downloaded the COVID-19 expression quantitative trait loci (eQTL) dataset (accession code: hum0343.v2) from the National Bioscience Database Center Human Database and

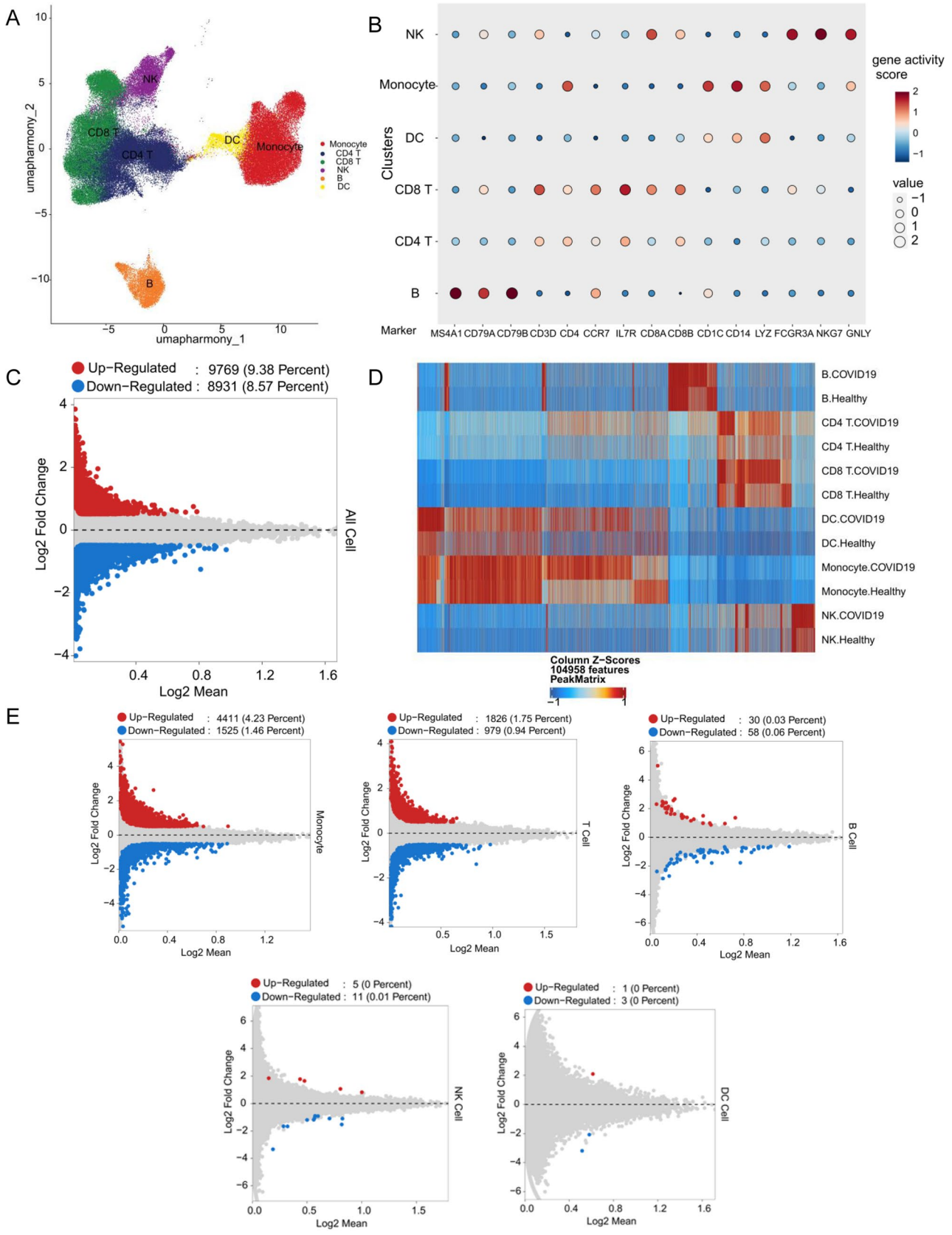
A
umapharmony_2
umapharmony_1
NK
CD8 T
CD4 T
DC
Monocyte
B
Monocyte
CD4 T
CD8 T
NK
B
DC
B
Clusters
NK
Monocyte
DC
CD8 T
CD4 T
B
Marker
MS4A1 CD79A CD79B CD3D CD4 CCR7 IL7R CD8A CD8B CD1C CD14 LYZ FCGR3A NKG7 GNLY
gene activity score
value
C
Up-Regulated : 9769 (9.38 Percent)
Down-Regulated : 8931 (8.57 Percent)
Log2 Fold Change
Log2 Mean
All Cell
D
B.COVID19
B.Healthy
CD4 T.COVID19
CD4 T.Healthy
CD8 T.COVID19
CD8 T.Healthy
DC.COVID19
DC.Healthy
Monocyte.COVID19
Monocyte.Healthy
NK.COVID19
NK.Healthy
Column Z-Scores
104958 features
PeakMatrix
E
Up-Regulated : 4411 (4.23 Percent)
Down-Regulated : 1525 (1.46 Percent)
Monocyte
Up-Regulated : 1826 (1.75 Percent)
Down-Regulated : 979 (0.94 Percent)
T Cell
Up-Regulated : 30 (0.03 Percent)
Down-Regulated : 58 (0.06 Percent)
B Cell
Up-Regulated : 5 (0 Percent)
Down-Regulated : 11 (0.01 Percent)
NK Cell
Up-Regulated : 1 (0 Percent)
Down-Regulated : 3 (0 Percent)
DC Cell

◂**Fig. 1** Altered chromatin accessibility in PBMCs from COVID-19 patients, with the most significant changes in monocytes. **A** UMAP dimplot showing clusters of six PBMC types from scATAC-seq data. **B** Dot plot of gene activity scores for marker genes annotating each cell type. **C** Volcano plot displaying DAPs of PBMCs in COVID-19 patients. **D** Heatmap showing marker peaks for each cell type under different conditions (COVID-19 or Health). **E** Volcano plots of DAPs for monocytes, T cells, B cells, NK cells or DC cells. Monocytes exhibit the most significant changes, mainly up-regulations

used the taskforce_rna_ releasedata_cis_eqtls.tsv.gz file [24]. Genomic locations of open chromatin peaks were considered to be associated with eQTLs if they overlapped with at least one cis-eQTL (p-value < 0.05).

Co-IP and ChIP-qPCR

Differentially treated THP-1 cells were lysed with cell lysate supplemented with protease inhibitors. The supernatant was centrifuged and collected, and a part of it was regarded as input. For co-immunoprecipitation (Co-IP), immunoprecipitation buffer containing IP antibody-conjugated magnetic beads (Biolinkedin, CHN) was used to immunoprecipitate the lysate from 1×10^7 THP-1 cells, and the complexes of magnetic beads-antibody-protein were washed with the lysis buffer and separated by a magnetic separator rack (Millipore, USA). Then the protein–protein complexes were then subjected to Western blotting. The protein bands were visualized using the ChemiDoc XRS + Imaging System (Bio-rad, USA) system. IgG was used here as a negative control.

For chromatin immunoprecipitation (ChIP)-qPCR, the DNA preparation, the cross-linking, and immunoprecipitation were conducted following the instructions provided by manufacturers using ChIP Assay Kit (ABclonal, CHN). One million cells per sample were used, and sonication was performed using Scientz ultrasonic cell crusher with a 5 s on—5 s off routine for a total of ~ 15 min on ice to obtain fragments size between 100–800 bp. The samples were then subjected to qPCR with indicated primers. Data were normalized to the IgG control group.

RT-qPCR and Western blotting

Using the Trizol (Beyotime, CHN) to extract total RNA following the instructions. cDNA synthesis was undertaken with the ABS Script II RT Mix (ABclonal, CHN). The 2× Universal SYBR Green Fast qPCR Mix (ABclonal, CHN) as well as primer sets were utilized for real-time qPCR. Fluorescence signals were detected using the CFX96 Touch PCR system (Bio-Rad, USA), with transcript levels measured by the $2-\Delta\Delta Ct$ method. Data was normalized against GAPDH.

Proteins from THP-1 cells under different treatments were isolated using RIPA lysis buffer. Protein samples were separated by SDS-PAGE, then transferred onto a PVDF membranes. The membranes were blocked with 5% non-fat milk for 60 min, followed by incubation with anti-JUND and anti-SMARCC1 antibodies. HRP-conjugated secondary antibody (H + L) was purchased from ABclonal (CHN). The immunoreactive bands were detected by the ChemiDoc XRS + imaging system (Bio-rad, USA). Correlation signals were quantified by Image J software.

Immunofluorescence and confocal imaging

THP-1 cells were seeded into cell culture dishes with round climbing slides and centrifuged to adhere. Cells were then fixed with 4% paraformaldehyde, permeabilized using absolute ethanol, and blocked with TBST (3% BSA) for 1 h. For localization of SMARCC1, cells were incubated with Tubulin and SMARCC1 primary antibodies overnight at 4 °C. For the co-localization of SMARCC1 and H3K27ac, cells were incubated at 4 °C overnight with blocking buffer containing SMARCC1 and H3K27ac primary antibodies. The nonspecific-binding antibodies were removed by PBS, and the cells were incubated with blocking buffer containing a fluorescent dye-conjugated secondary antibody. DAPI was used to counterstain the nuclei. Scanning and imaging were used FV3000 confocal laser scanning microscope (Olympus, JPN). Image quantification was performed in ImageJ (Fiji).

Statistical analyses

For all the bar graphs, data were presented as mean ± standard deviation (SD). Statistical analyses were performed with two-tailed Student's t test or one-way ANOVA using GraphPad Prism 9. $p < 0.05$ was considered statistically significant ($*p < 0.05$, $**p < 0.01$, $***p < 0.001$, $**** p < 0.0001$).

Results

Monocytes exhibited the most significant changes in chromatin accessibility in COVID-19 patients

We collected scATAC-seq data of PBMCs from COVID-19 patients and healthy individuals to explore the altered epigenetic profiles of immune cell populations. Utilizing the R packages ArchR and scOpen for analysis, we conducted quality control on the scATAC-seq data, and clustered a total of 100,347 cells into six distinct PBMC subpopulations (Fig. 1A). Gene activity scores were calculated based on the accessibility within three key genomic regions associated with each gene: promoter, gene bodies, and distal regulatory

elements. These gene activity scores of canonical markers were used to annotate the six cell clusters. The cell clusters were defined as $CD8^+$ T cells, $CD4^+$ T cells, B cells, natural killer (NK) cells, monocytes, and dendritic cells (DC). The gene activity scores for cell markers in each cluster were presented in Fig. 1B.

We performed peak calling and marker peak detection on scATAC-seq data. The chromatin accessibility of PBMCs in COVID-19 patients was significantly altered compared to healthy individuals, with 9,769 out of 104,193 reproducible peaks showing increased accessibility in COVID-19 patients (Fig. 1C). When comparing peak accessibility between COVID-19 and healthy people within each cell clusters, we found that monocytes exhibited the most pronounced changes in chromatin accessibility among the PBMCs, followed by T cells (Fig. 1D and E). These data suggest that COVID-19 monocytes are activated and undergo extensive chromatin remodeling, leading to significantly altered chromatin accessibility landscapes.

Increased chromatin accessibility of pro-inflammatory cytokines in COVID-19 monocytes

Next, we performed sub-clustering of monocytes in the scATAC-seq data. Unsupervised clustering identified eight epigenetically distinct cell clusters, with clusters C2 and C3 predominantly comprising cells from healthy individuals (Fig. 2A). We conducted a comprehensive analysis of the open chromatin regions in monocytes and identified marked disparities in chromatin accessibility between COVID-19 patients and healthy individuals. Specifically, 5,479 DAPs showed increased accessibility in patients, while 1,918 DAPs showed decreased accessibility compared to healthy controls (Fig. 2B). Among the 5,479 DAPs located in open chromatin regions in COVID-19 monocytes, 9% were in promoter regions, 48% in introns, and 36% in distal regions (Fig. 2C).

We annotated genes adjacent to the DAPs. Subsequently, enrichment analyses were performed on the nearest genes of DAPs to decipher their functional roles. GO analysis highlighted cholesterol/sterol pathway and immune-related processes in monocytes from COVID-19 patients, including leukocyte migration, regulation of immune effector processes, positive regulation of inflammatory response, and cytokine-mediated signaling pathways (Fig. 2D). KEGG analysis highlighted cytokine-cytokine receptor interaction, chemokine signaling, MAPK signaling, NF-kB signaling, choline metabolism and inositol phosphate metabolism (Fig. 2E). These results indicate that the increased chromatin accessibility in COVID-19 monocytes might regulate the expression of pro-inflammatory cytokines and drive inflammatory responses.

We used the 'plotBrowserTrack' function in ArchR to generate genome browser tracks, visualizing gene accessibility profiles under different conditions. Genome browser tracks revealed significantly higher chromatin accessibility of pro-inflammatory cytokines IL-6, TIMP1, CX3CR1, CCR2, CCL2, and S100A9 in COVID-19 patients (Fig. 2F). These findings suggest that the chromatin landscape in COVID-19 monocytes undergoes substantial alterations, particularly with increased accessibility of inflammation-related genes, potentially linked to disease progression.

Combined analysis of scATAC-seq and scRNA-seq indicated potential epigenetic regulation of the expression of pro-inflammatory cytokines

Integrating analyses of scATAC-seq and scRNA-seq data from COVID-19 patients and healthy individuals were performed to investigate the connection between epigenetic changes and alterations in gene expression. Unsupervised clustering of PBMCs identified six cell types based on marker genes in the scRNA-seq dataset (Fig. 3A). Subsequent re-clustering of monocytes in the scRNA-seq data revealed eight distinct clusters, with the seventh cluster (designated as R7) primarily comprising COVID-19 monocytes (Fig. 3B). Compared to healthy controls, the expression of inflammatory cytokines including TIMP1, CCR2, CCR1, CCL2, CX3CR1, IL-16, S100A6, and S100A8, etc., increased in monocytes from patients (Fig. 3C). Notably, expression changes of TIMP1, CCL2, CCR1/2, CX3CR1 and S100A6 were consistent with alterations in their chromatin regions respectively (Fig. 2F and 3C).

DEGs of monocytes from scRNA-seq data were further identified and cross-referenced with DAPs from scATAC-seq data. Among the 2,208 DEGs identified in monocytes, 1,617 genes (73.23%) exhibited consistent changes (1450 up-regulated genes and 167 down-regulated) in both scRNA-seq and scATAC-seq data (Fig. 3D). We further calculated a gene score matrix from scATAC-seq data to assess the correlation between gene scores and expression levels measured by scATAC-seq and scRNA-seq, respectively. Analyzing accessibility of peaks within 1 Mb of gene promoters with gene expression, we identified a total of 111,173 peak-to-gene correlations in different monocyte populations (Fig. 3E). These peak-to-gene links likely play a crucial role in gene regulation, as evidenced by the strong consistency revealed in the integrated analysis of scATAC-seq and scRNA-seq datasets from COVID-19 monocytes. The high degree of overlap between chromatin accessibility and gene expression in our data suggests that transcriptional responses are likely modulated by epigenetic changes.

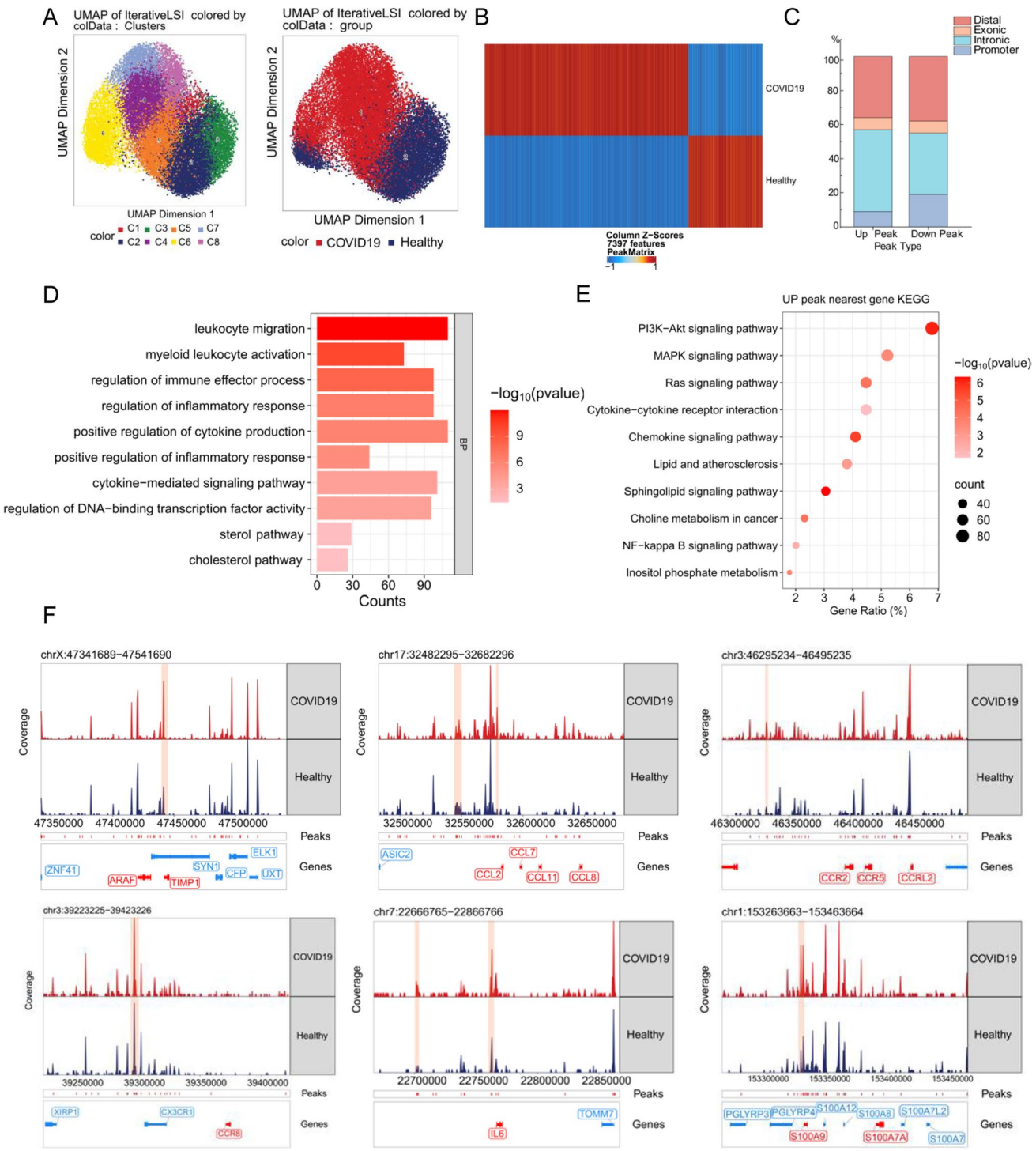

Fig. 2 scATAC-seq analysis reveals increased chromatin accessibility for pro-inflammatory cytokines in COVID-19 monocytes. **A** Monocytes in the scATAC-seq dataset were subset and re-clustered. Left panel showing 8 unsupervised clusters; right panel showing the distribution of monocyte under COVID-19 or health, respectively. **B** Heatmap showing marker peaks in monocytes from patients and healthy individuals. **C** Bar graph displaying the distribution of DAPs mapped to exon, intron, promoter, and distal intergenic regions in COVID-19 monocytes. **D** Enriched GO biological processes terms for genes nearest to differentially upregulated accessible peaks. **E** Enriched KEGG pathways for genes nearest to differentially upregulated accessible peaks. **F** Genome browser tracks showing single-cell chromatin accessibility at representative gene loci (TIMP1, CCL2, CCR2, CX3CR1, S100A9 and IL-6) with peaks and gene information indicated below

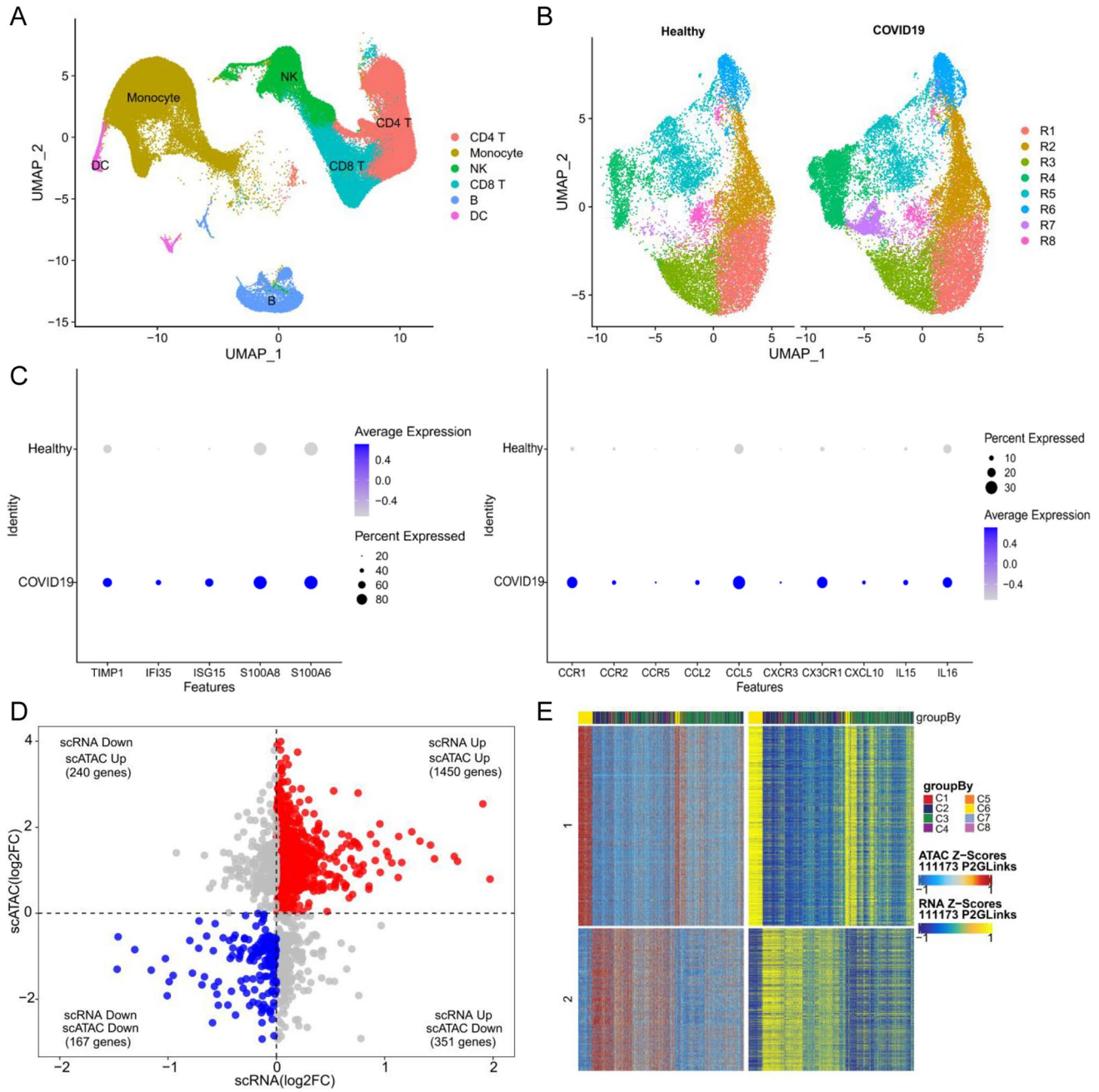

Fig. 3 The transcriptional profiles of pro-inflammatory cytokines align with their chromatin accessibility status in COVID-19 monocytes. **A** UMAP dimplot showing six PBMC cell type clusters from scRNA-seq. **B** UMAP plot displaying monocyte sub-clusters distribution under COVID-19 or healthy conditions in scRNA-seq data. **C** Dot plots showing gene expression for the specified genes in monocytes. Left panel, TIMP1, alarmins and interferon family genes; right panel, chemokines and interleukins. **D** Scatterplots depicting the DEGs and DAPs identified in monocytes across COVID-19 patients and healthy individuals. **E** Heatmaps showing the column z-score of normalized accessibility and integrated gene expression of 111,173 peak-to-gene links in monocytes across the subclusters. Each row represents a cis-regulatory element-linked gene pair

Collaborative regulation of pro-inflammatory cytokines by the chromatin remodeling complex subunit SMARCC1 and transcription factor JUND

To elucidate the epigenetic regulatory characteristics of gene expression in COVID-19 monocytes, we conducted motif-enrichment analysis on highly accessible chromatin regions for TFs. Among the identified regions, we discovered 75 TFs with significantly enriched motifs (mlog10 Padj > 5), including SMARCC1, JUND, JUNB, FOS, FOSL1/FOSL2. Notably, JUND, JUNB, FOS and FOSL1/FOSL2, all AP-1 family members, exhibited significantly higher enrichment levels in patients compared to healthy individuals (Fig. 4A). Given the key roles of these factors in inflammation, we investigated their expression levels in relation to the accessibility changes in their corresponding motifs. We first constructed MotifMatrix based on deviation z-scores and chromVAR deviations for each TF motif in healthy and patient groups to quantify the variability in motif accessibility. Subsequently, MotifMatrix and GeneSoreMatrix were used to identify TFs whose motif accessibility correlated with their own gene activity. Additionally, the maximum delta deviation in z-scores across groups was calculated to help stratify motifs based on their variation degree. Those analyses revealed that JUND, FOS, FOSL1/FOSL2 and SMARCC1 are positive regulators as their expression levels were positively correlating with the accessibility changes of the respective motifs (Fig. 4B).

ChromVAR was employed to measure global TF activity and assess key TFs across cell clusters. The activity of SMARCC1 and JUND regulatory elements across different monocyte clusters was shown in Fig. 4C. Interestingly, we found the consistent pattern in SMARCC1 and JUND activity across monocyte clusters, particularly upregulated in C4 and C7, which were predominantly composed of cells from COVID-19 patients.

SMARCC1, as a core subunit of the SWI/SNF chromatin remodeling complex, plays a vital role in chromatin remodeling processes. To explore the relationship between SMARCC1 and JUND, we analyzed the binding motif for both factors and generated sequence logo diagrams (Fig. 4D). The binding motifs of these regulatory elements were largely consistent, both containing the nucleotide alphabet 'TGACTCA'. Next, we extracted the peaks matched by SMARCC1 and JUND motifs respectively and found their intersection, the results revealed that SMARCC1 and JUND shared 68.1% common binding sites, implying a potential co-operative effect (Fig. 4D).

Based on the nearest genes of motif-matched peaks, we further investigated the interaction between these regulatory elements and their targets genes. A total of 6,498 genes were identified as nearest genes of co-matched peaks by JUND and SMARCC1 motifs, of which 986 genes showed upregulation in monocytes from patients compared to healthy individuals in both scATAC-seq and scRNA-seq datasets (Fig. 4E). GO biological process (BP) analysis showed that these genes were associated with inflammation, cytokine production and sterol pathway (Fig. 4F). This suggests that SMARCC1 and JUND may cooperatively regulate gene expression, and involved in sterol signals and proinflammatory cytokine production. Interestingly, the pro-inflammatory cytokine TIMP1 was associated with peaks harboring both JUND and SMARCC1 motifs (Fig. 4G), indicating that JUND and SMARCC1 may synergistically regulate TIMP1 expression.

eQTLs combined with scATAC-seq analyses revealed SNP enrichment in open chromatin regions with regulatory potentials

Previous genomic studies have identified numerous risk factors for COVID-19, primarily in intergenic regions [24]. eQTLs are genetic variants that regulate gene expression and link genotype to phenotype, primarily single nucleotide polymorphisms (SNPs) [25]. We utilized COVID-19 specific cis-expression quantitative trait loci (cis-eQTLs) data to assess if these regulatory variants were in the open chromatin regions of monocytes. By integrated analyses of the COVID-19 cis-eQTLs with monocyte scATAC-seq peaks, we discovered that 60.9% of highly accessible peaks in COVID-19 monocytes contained eQTLs. Specifically, 29.1% of SNPs were located in intronic peaks, while 22.3% were found in distal regions, consistent with the majority of eQTLs in non-coding regions (Fig. 5A). In comparison, 57.4% of down-regulated peaks in COVID-19 monocytes contained eQTLs (Fig. 5B). In particular, the chromatin regions harboring SMARCC1 and JUND motifs had a high proportion (> 60%) containing eQTLs (Fig. 5C). These results provided genetic evidence that accessible peaks with eQTLs are most likely involved in regulating gene expression.

We further investigated the COVID-19 cis-eQTLs mapping for inferred peak-to-gene links and discovered an enrichment of cis-eQTLs variants within these links. In monocytes, variants rs57008264 and rs9990343, which potentially regulate CCR1 expression, were found within an accessible chromatin peak and associated with the CCR1 transcript levels. Additionally, we observed that variants rs13069750, rs34340501, and rs34724655, were located within open chromatin peaks and associated with CCR2 expression (Fig. 5D). These findings indicate that these cis-eQTLs variants may influence the gene expression by altering chromatin accessibility or TF binding.

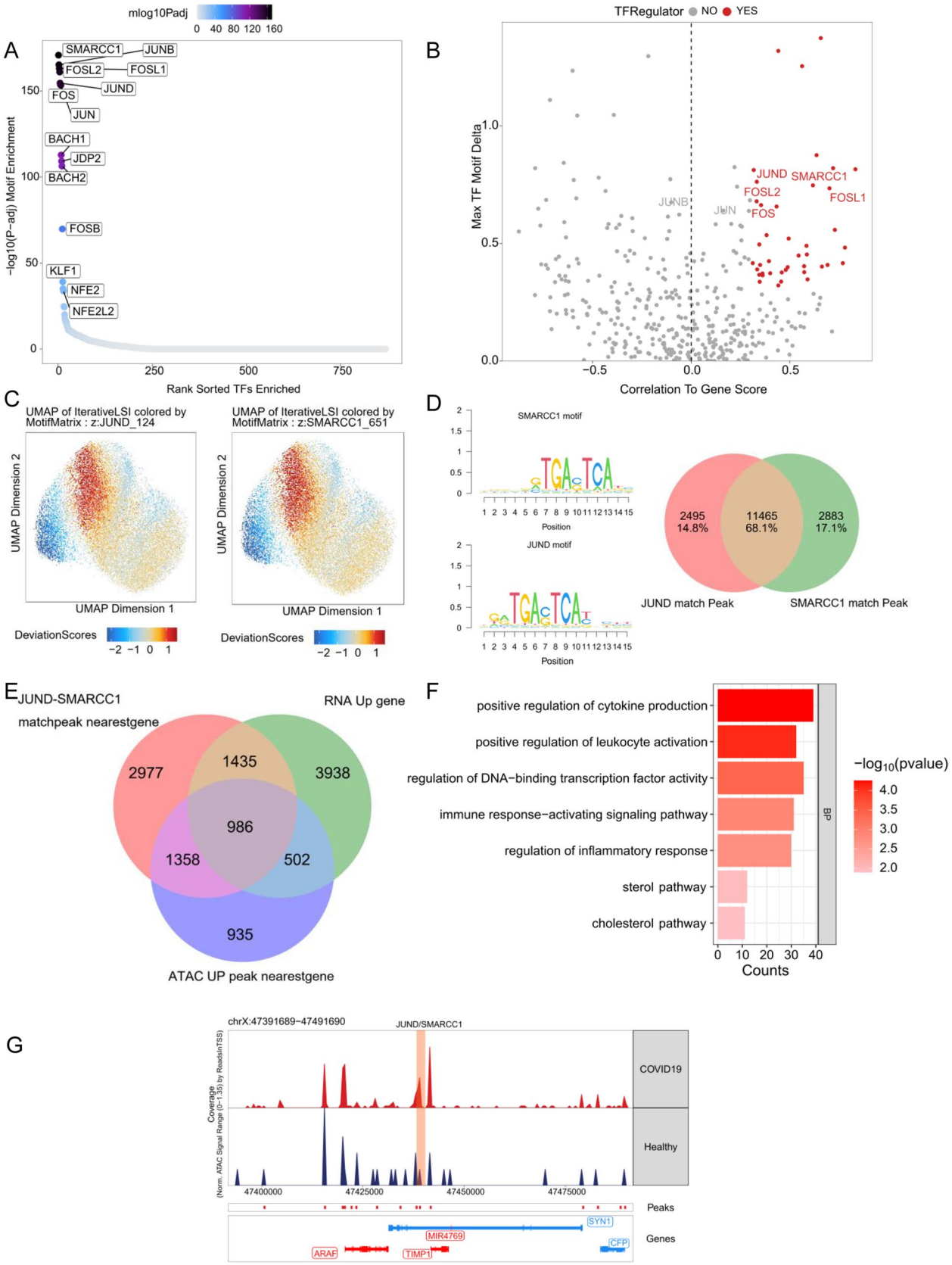
A
mlog10Padj
0 40 80 120 160
SMARCC1
JUNB
FOSL2
FOSL1
FOS
JUND
JUN
BACH1
JDP2
BACH2
FOSB
KLF1
NFE2
NFE2L2
−log10(P−adj) Motif Enrichment
Rank Sorted TFs Enriched
B
TFRegulator NO YES
Max TF Motif Delta
Correlation To Gene Score
JUND
SMARCC1
FOSL2
FOSL1
JUNB
JUN
FOS
C
UMAP of IterativeLSI colored by MotifMatrix : z:JUND_124
UMAP of IterativeLSI colored by MotifMatrix : z:SMARCC1_651
UMAP Dimension 1
UMAP Dimension 2
DeviationScores
D
SMARCC1 motif
JUND motif
Position
2495
14.8%
11465
68.1%
2883
17.1%
JUND match Peak
SMARCC1 match Peak
E
JUND-SMARCC1
matchpeak nearestgene
RNA Up gene
ATAC UP peak nearestgene
2977
1435
3938
986
1358
502
935
F
positive regulation of cytokine production
positive regulation of leukocyte activation
regulation of DNA−binding transcription factor activity
immune response−activating signaling pathway
regulation of inflammatory response
sterol pathway
cholesterol pathway
BP
−log10(pvalue)
Counts
G
chrX:47391689−47491690
JUND/SMARCC1
COVID19
Healthy
Peaks
Genes
SYN1
MIR4769
CFP
ARAF
TIMP1

◂**Fig. 4** SMARCC1 and JUND synergistically regulate gene transcriptional profiles in monocytes. **A** Rank sorted TFs enriched in COVID-19 monocytes compared to healthy individuals. **B** Volcano plot of positive TF regulators depicting TFs whose inferred gene scores are positive correlated to accessibility changes observed in their corresponding motifs. Positive TFs are highlighted in red. **C** UMAP plots illustrating chromVAR deviation z-scores for JUND (left) and SMARCC1 (right). **D** Venn diagram showing the overlap among co-matched peaks of JUND and SMARCC1 motifs. The left side panels show the sequence logo of the JUND motif and SMARCC1 motif. **E** Venn diagram displaying the intersection of upregulated genes, nearest genes of upregulated accessible peaks and nearest genes of co-matched SMARCC1/JUND motif peaks in monocytes. Genes from the intersection are potentially co-regulated by JUND and SMARCC1. **F** GO BP enrichment analysis of genes from intersections in (E). **G** Genome browser tracks displaying chromatin accessibility at TIMP1 locus in monocyte under different conditions. Shaded areas indicate potential JUND/SMARCC1 binding sites. Peaks and gene information are indicated below the tracks

The metabolite 7α,25-OHC promoted the expression of proinflammatory cytokine TIMP1 in THP-1 cell line

7α,25-OHC is generated from the metabolism of 25-hydroxycholesterol by cytochrome P450 family 7 subfamily B member 1 (CYP7B1) (Fig. 6A). In COVID-19 patients, serum levels of 7α,25-OHC were elevated, and transcriptome sequencing data also indicated the increase in CYP7B1 expression in peripheral blood (Fig. 6B). Previous pathway enrichment analysis showed that the nearest genes of DAPs in COVID-19 monocytes enriched in cholesterol-related pathways (Fig. 2D). To investigate whether 7α,25-OHC is involved in the production of inflammatory cytokines in monocytes, we stimulated THP-1 cells with 7α,25-OHC. THP-1 is a human monocytic cell line, which serves as a common model for studying monocyte and macrophage activity modulation. In vitro stimulation of monocytes with 7α,25-OHC induced significant transcriptome changes and upregulated pro-inflammatory cytokines, including TIMP1, CCR1, and CX3CR1, etc., in a 7α,25-OHC concentration-dependent manner (Fig. 6C). Using NIBR189, an antagonist of G Protein-Coupled Receptor 183 (GPR183), to block the binding of 7α,25-OHC to its receptor (GPR183), the expression of TIMP1 induced by 7α,25-OHC was significantly downregulated (Fig. 7C).

In-vitro experiments indicated that SMARCC1 interacted with JUND to co-regulate TIMP1 expression

To verify the interaction between JUND and SMARCC1, we performed immunoprecipitation and Western blot with JUND and SMARCC1 antibody, respectively. Co-IP confirmed the interaction between SMARCC1 and JUND, suggesting a potential cooperation in the regulation of gene expression (Fig. 6D). ChIP-qPCR experiment further confirmed that the expression of TIMP1 was regulated by JUND (Fig. 6E).

Western blot analysis demonstrated a concentration-dependent increase of the TF JUND and the chromatin remodeling complex core subunit SMARCC1 in THP-1 cells treated with 7α,25-OHC (Fig. 7A and B). When the interaction of 7α,25-OHC with its receptor GPR183 was blocked using a GPR183 antagonist, the protein levels of JUND and SMARCC1 significantly reduced (Fig. 7D). Immunofluorescence and confocal imaging revealed that SMARCC1 is predominantly located in the nucleus, and 7α,25-OHC treatment intensified SMARCC1 nuclear fluorescence in a concentration-dependent manner (Fig. 7E. S1 A and S1B).

7α,25-OHC enhanced the expression and co-localization of SMARCC1 and H3K27ac

7α,25-OHC stimulation promoted histone acetylation and SMARCC1 expression with concentration-dependent manner in THP-1 cells (Fig. 7A, S1C and S1E). Immunofluorescence and laser confocal imaging further demonstrated that 7α,25-OHC enhanced SMARCC1 and acetylated H3K27 co-localization (Fig. S1C and S1D). Based on our findings, the inflammatory metabolite 7α,25-OHC enhances JUND and SMARCC1 expression, and facilitates the H3K27ac and its co-localization with SMARCC1 in a concentration-dependent manner in THP-1.

Discussion

Cell-specific epigenetic elements play an important role in the molecular pathogenesis of infectious diseases, autoimmune diseases, tumors and others [16]. Giroux NS et al. revealed that individual PBMC cell types exhibit evolution of the chromatin accessibility landscape, and monocytes are the major cell type differentially activated [19]. Our study indicated that monocytes underwent significant chromatin remodeling, with the core subunit of the chromatin remodeling complex SMARCC1 and TF JUND co-modulating the expression of the pro-inflammatory cytokine TIMP1, and enhancing the inflammatory responses in COVID-19 patients. In-vitro experiments further demonstrated that high level of metabolite 7α,25-OHC enhanced the expression of JUND, SMARCC1, and H3K27ac to promote TIMP1 expression, which contribute to inflammatory responses in COVID-19.

Recent studies have identified TIMP1 as a significant inflammatory cytokine associated with various diseases, including viral infections, inflammatory bowel disease, osteoarthritis, and cancer [5]. Constitutively upregulation of TIMP1 inhibits ADAM10-mediated Notch signaling

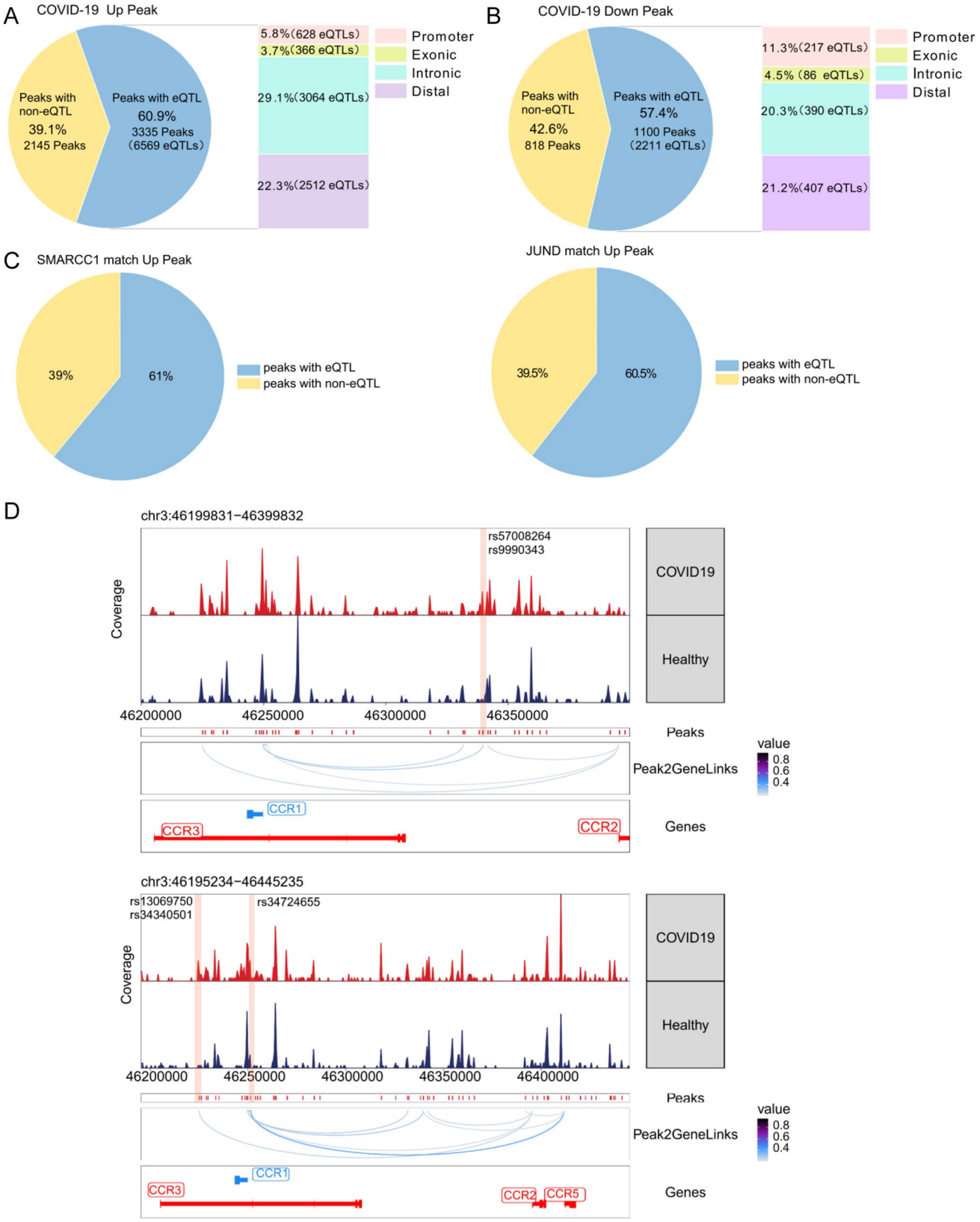
A
COVID-19 Up Peak
Peaks with non-eQTL
39.1%
2145 Peaks
Peaks with eQTL
60.9%
3335 Peaks
(6569 eQTLs)
5.8%(628 eQTLs)
3.7%(366 eQTLs)
29.1%(3064 eQTLs)
22.3%(2512 eQTLs)
Promoter
Exonic
Intronic
Distal
B
COVID-19 Down Peak
Peaks with non-eQTL
42.6%
818 Peaks
Peaks with eQTL
57.4%
1100 Peaks
(2211 eQTLs)
11.3%(217 eQTLs)
4.5% (86 eQTLs)
20.3%(390 eQTLs)
21.2%(407 eQTLs)
Promoter
Exonic
Intronic
Distal
C
SMARCC1 match Up Peak
39%
61%
peaks with eQTL
peaks with non-eQTL
JUND match Up Peak
39.5%
60.5%
peaks with eQTL
peaks with non-eQTL
D
chr3:46199831−46399832
rs57008264
rs9990343
Coverage
COVID19
Healthy
46200000
46250000
46300000
46350000
Peaks
Peak2GeneLinks
value
0.8
0.6
0.4
CCR1
CCR3
CCR2
Genes
chr3:46195234−46445235
rs13069750
rs34340501
rs34724655
Coverage
COVID19
Healthy
46200000
46250000
46300000
46350000
46400000
Peaks
Peak2GeneLinks
value
0.8
0.6
0.4
CCR1
CCR3
CCR2
CCR5
Genes

◂**Fig. 5** eQTLs are located in open chromatin regions of monocytes and can influence gene expression. **A** and **B** Cis-eQTLs in the differentially upregulated (A) and downregulated (B) accessible peaks of COVID-19 monocytes. Left panel, the proportion of cis-eQTLs in the DAPs; right panel, the distribution of the cis-eQTLs locations annotated to different genomic regions. **C** Pie charts showing the proportion of differentially upregulated peaks matched SMARCC1 and JUND motifs that contain cis-eQTLs. **D** Genome browser tracks showing potential cis-eQTLs associated with CCR1/CCR2 expression located in open chromatin peaks from scATAC-seq data. Shaded areas indicate cis-eQTLs loci. Peaks identified in the scATAC-seq data, peak-to-gene links and gene information are indicated below the tracks

pathways, which result in long-term myeloid-biased inflammatory hematopoiesis [26]. Zhao et al. demonstrated that elevated levels of TIMP1 in inflammatory malignancies promote the progression of malignant pleural effusion [27]. Benjamin Schoeps et al. reported that TIMP1 interacts with its receptor CD63, which activates the ERK pathway, triggering the formation of neutrophil extracellular traps, and promotes the progression of pancreatic cancer [28].

Our findings indicated that the accessibility of genomic chromatin regions (including promoter and enhancer regions) and the expression levels of pro-inflammatory cytokines, such as TIMP1, increased in monocytes from COVID-19 patients. The inflammatory metabolite 7α,25-OHC significantly increased in COVID-19 patients, and in vitro experiments demonstrated that 7α,25-OHC stimulated monocytes to produce pro-inflammatory cytokines, including TIMP1, and CCR1, etc.

SMARCC1, SMARCC2, and SMARCA4/SMARCA2 constitute the core subunits of the chromatin remodeling complex SWI/SNF (three variants of cBAF, ncBAF and PBAF) [29, 30]. SWI/SNF induced the exhaustion of $CD8^+$ T cells by directing chromatin accessibility and enhancing the expression of exhaustion associated genes such as TOX and ENTPD1, while the inhibition or degradation of SMARCA4 attenuated the exhaustion of $CD8^+$ T cells [31]. Upon inflammatory stimulation, SWI/SNF complexes in macrophages interact with stimulus-responsive TFs of the NF-kB family to promote the TNF response and the expression of inflammatory genes [32].

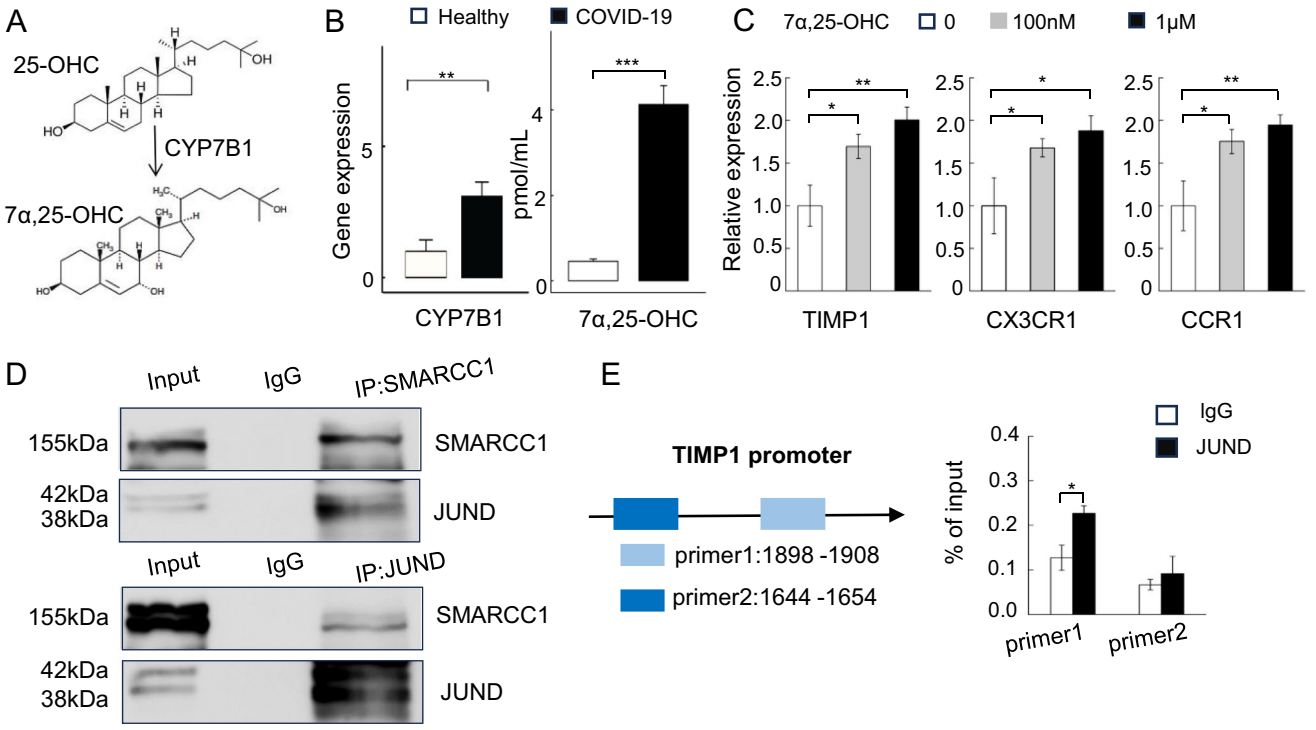

Fig. 6 Interaction between JUND and SMARCC1 in the regulation of TIMP1 expression. **A** Diagram illustrating the metabolic conversion of 25-OHC to 7α,25-OHC. **B** The bar charts displaying the expression levels of CYP7B1 enzyme (GSE206263) and 7α,25-OHC in the blood of COVID-19 patients. **C** mRNA levels of TIMP1, CCR1 and CX3CR1 were analyzed by qPCR. **D** The physical interaction between SMARCC1 and JUND was validated by Co-IP and Western blotting. **E** Regulation of TIMP1 transcription by JUND. Left panel, potential binding sites of TF JUND on the TIMP1 promoter sequence; right panel, ChIP-qPCR detects JUND binding to the TIMP1 promoter, with IgG as negative control. Experiment repeated independently at least three times. Data are shown as the mean ± SD and statistical analysis performed using two-tailed Student's t test (Fig. 6B and E) or one way ANOVA (Fig. 6C). $*p < 0.05$, $**p < 0.01$, $***p < 0.001$

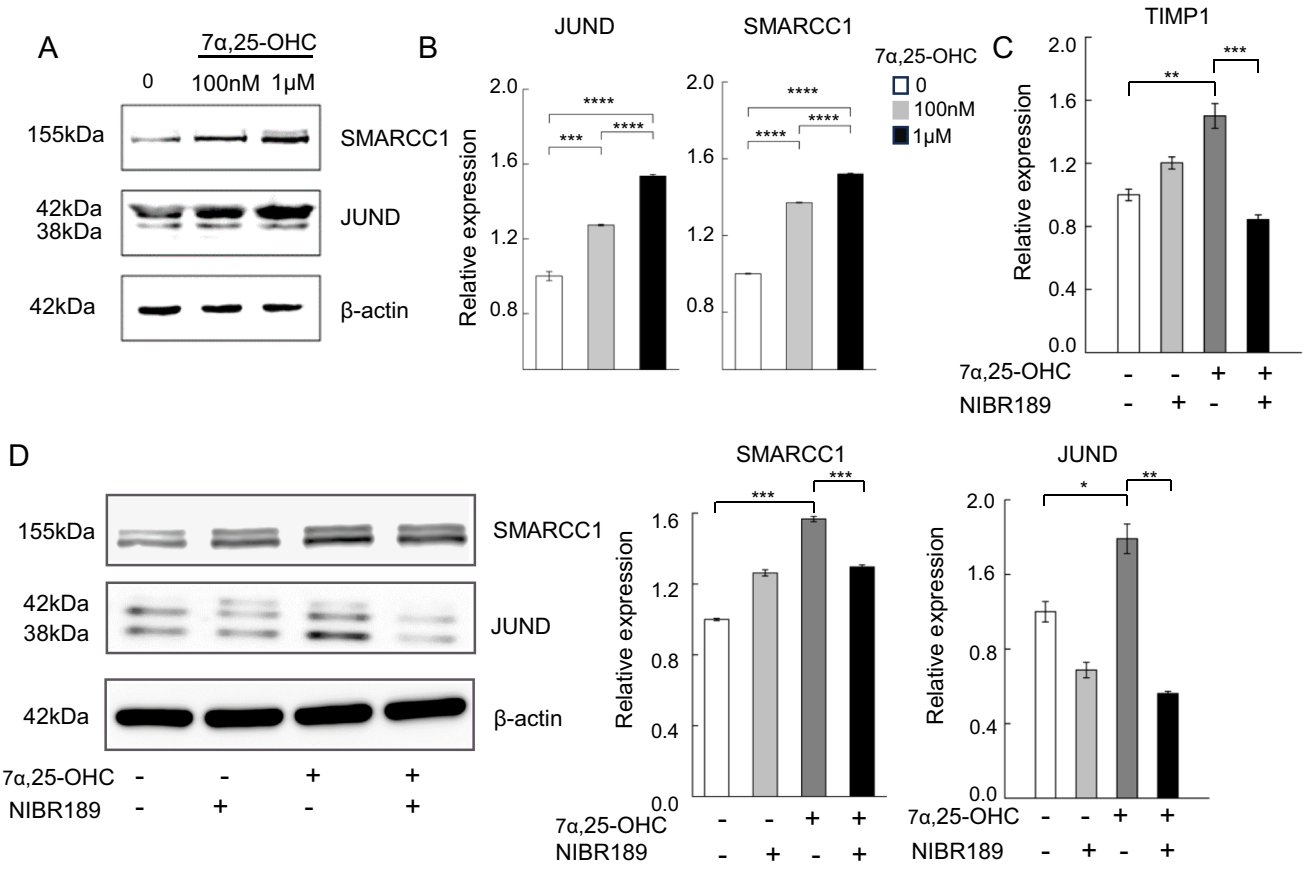
A
7α,25-OHC
0
100nM
1μM
155kDa
SMARCC1
42kDa
38kDa
JUND
42kDa
β-actin
B
JUND
SMARCC1
7α,25-OHC
0
100nM
1μM
Relative expression
C
TIMP1
Relative expression
7α,25-OHC
NIBR189
D
155kDa
SMARCC1
42kDa
38kDa
JUND
42kDa
β-actin
7α,25-OHC
NIBR189
SMARCC1
JUND
Relative expression

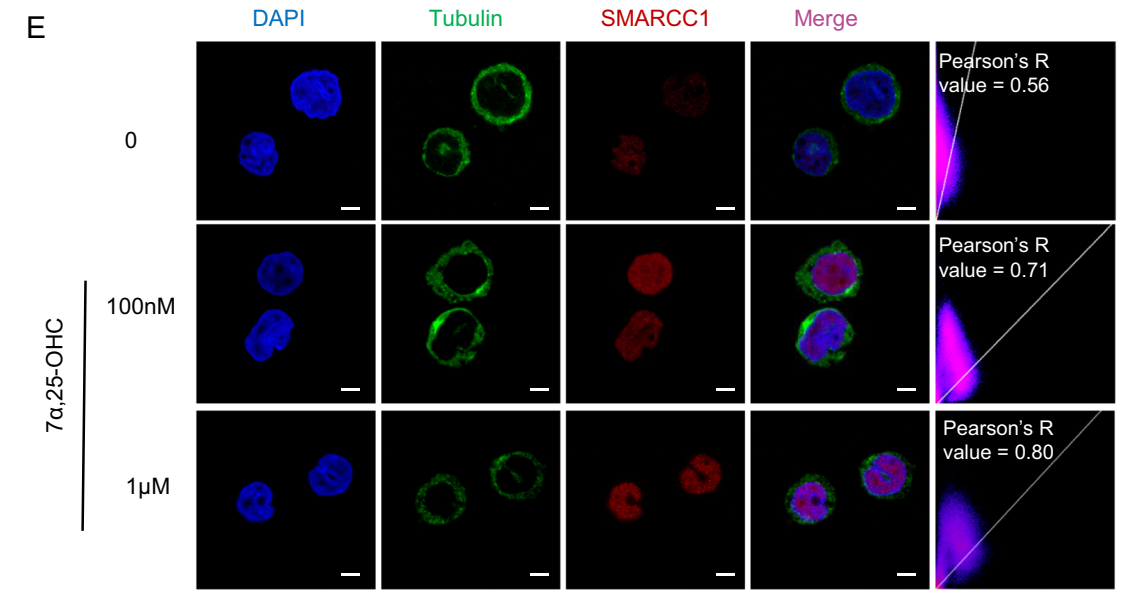
E
DAPI
Tubulin
SMARCC1
Merge
0
100nM
1μM
7α,25-OHC
Pearson's R value = 0.56
Pearson's R value = 0.71
Pearson's R value = 0.80

◂**Fig. 7** 7α,25-OHC upregulates JUND and SMARCC1 expression, and nuclear accumulation of SMARCC1 in THP-1 cells. **A** The levels of SMARCC1 and JUND proteins were assessed by Western blot after treatment with 0,100 nM or 1 μM 7α,25-OHC for 18 h. **B** Relative intensities of JUND and SMARCC1 protein in (A) were quantified using ImageJ. **C** mRNA levels of TIMP1 were analyzed by qPCR. **D** The levels of SMARCC1 and JUND proteins were assessed by Western blot after treatment with 0; 1 μM NIBR189 only; 1 μM 7α,25-OHC only; 1 μM NIBR189 and 1 μM 7α,25-OHC for 18 h. The right side panels showing relative intensities of JUND and SMARCC1 protein. **E** Immunofluorescence of SMARCC1 (red) in THP-1 cells treated with 100 nM/1 μM 7α,25-OHC for 18 h examined by confocal microscopy. DAPI (blue) and tubulin (green) were used to stain nuclei and cytoskeleton, respectively. Scale bar, 5 μm. Experiment repeated independently at least three times. Data are shown as the mean ±SD and statistical analysis performed using one way ANOVA (Fig. 7B, C and D). *$p < 0.05$, **$p < 0.01$, ***$p < 0.001$, **** $p < 0.0001$

In this study, the combined scATAC-seq and scRNA-seq analyses suggest that the transcription of the pro-inflammatory cytokines, including TIMP1, were epigenetically regulated in monocytes from COVID-19 patients, with significant enrichment of regulatory elements such as SMARCC1 and the AP-1 family member JUND. Subsequent investigation indicated that the chromatin regions are highly co-regulated by the core subunit of the SWI/SNF complex, SMARCC1, and TF JUND. Notably, the promoter region of the pro-inflammatory cytokine TIMP1 harbors binding motifs for both JUND and SMARCC1. Further experiments, Co-IP, and ChIP-qPCR, etc., indicated that an interaction between JUND and SMARCC1, which were involved in TIMP1 expression and inflammatory responses.

The chromatin accessibility and SWI/SNF activity can be affected by the methylation or acetylation of the histone lysine residues [30]. Previous studies have suggested that the SWI/SNF complexes cooperate and co-localize with Plant Homeodomain-like Finger protein 6 at the active promoters enriched for acetylation of histone H3 at Lysine 14 (H3K14ac) to modulate gene expression [33]. Our results indicated that monocytes stimulated with 7α,25-OHC increased the SMARCC1 expression and H3K27ac in a concentration dependent manner, and the co-localization of SMARCC1 and H3K27ac were validated using laser confocal experiments.

SWI/SNF remodels chromatin accessibility through reducing nucleosome occupancy or moving nucleosomes away from cis-motifs on enhancers; recent study also revealed that SWI/SNF facilitated further chromatin opening with acetylated histones [34, 35]. Our results indicated that 7α,25-OHC upregulated SMARCC1 and JUND expression, and enhanced SMARCC1 nuclear accumulation. JUND may recruited SMARCC1, the core subunit of chromatin remodeling complex SWI/SNF, to facilitate dynamic chromatin reorganization, which was involved in transcriptional expression of pro-inflammatory cytokine TIMP1 gene. Furthermore, SMARCC1-JUND transcriptional complex may further amplify epigenetic-transcriptional activity through recognition of H3K27ac chromatin regions.

In this study, utilizing the single-cell multi-omics methodology alongside in-vitro experiments, we demonstrated that high level of 7α,25-OHC in peripheral blood stimulated the overexpression of SMARCC1 and JUND in monocytes. SMARCC1 interaction with JUND, and SMARCC1 co-localization with H3K27ac loci may led to a synergistic remodeling effect, which facilitated the further opening of these chromatin regions, and enhanced the expression of TIMP1 and CCR1, etc. The transcriptional regulatory process triggered the inflammatory response of COVID-19. Our findings enhance the comprehension of the transcriptional regulatory mechanisms of inflammatory responses in COVID-19, and offer novel targets for the treatment of COVID-19.

Supplementary Information The online version contains supplementary material available at https://doi.org/10.1007/s00018-025-05721-w.

Author contributions Conceptualization, J.Z. and Z.-H.L.; Methodology, J.Z., Y.F., Z.W., H.Y., K.H., Z.-Y.W. and Z.-H.L.; Investigation and data analysis, Y.F., Z.W.,K.H., Y.W., J.L. and S.Y; Validation, Y.F., Z.W., S.Y., J.L. and Y.W; Visualization, Y.F., Z.W., K.F., Z.-Y.W., Y.W., and S.Y.; Writing—original draft, J.Z., Y.F., Z.W., Y.H. and Z.-H.L.; Writing—review and editing, J.Z., Y.H and Z.-H.L.; Supervision and funding acquisition, J.Z. and Z.H.L.; All authors have read and approved the published version of the manuscript.

Funding This study was funded by the Department of Science and Technology of Hubei Province (#2022EHB035) and the Hubei Chutian Program (#1180011).

Data availability The raw data used in this study is publicly available in the GEO database under the accession numbers GSE206283 and GSE206455. The data generated during the current study are available from the corresponding author on reasonable request.

Declarations

Ethics approval The investigations involving human participants have complied with all relevant ethical regulations. This study was reviewed and approved by Ethics Committee of Wuhan University of Science and Technology (#216).

Consent to participate Informed consent was obtained from all individual participants included in the study.

Consent to publish The authors affirm that human research participants provided informed consent for publication.

Competing interests The authors declare that they have no competing interests.

References

1. Davis HE, McCorkell L, Vogel JM, Topol EJ (2023) Long COVID: major findings, mechanisms and recommendations. Nat Rev Microbiol 21(3):133–146. https://doi.org/10.1038/s41579-022-00846-2
2. Peluso MJ, Deeks SG (2024) Mechanisms of long COVID and the path toward therapeutics. Cell 187(20):5500–5529. https://doi.org/10.1016/j.cell.2024.07.054
3. Zhang HP, Sun YL, Wang YF, Yazici D, Azkur D, Ogulur I et al (2023) Recent developments in the immunopathology of COVID-19. Allergy 78(2):369–388. https://doi.org/10.1111/all.15593
4. Nazerian Y, Ghasemi M, Yassaghi Y, Nazerian A, Hashemi SM (2022) Role of SARS-CoV-2-induced cytokine storm in multi-organ failure: Molecular pathways and potential therapeutic options. Int Immunopharmacol 113(Pt B):109428. https://doi.org/10.1016/j.intimp.2022.109428
5. Schoeps B, Frädrich J, Krüger A (2023) Cut loose TIMP-1: an emerging cytokine in inflammation. Trends Cell Biol 33(5):413–426. https://doi.org/10.1016/j.tcb.2022.08.005
6. Landy E, Carol H, Ring A, Canna S (2024) Biological and clinical roles of IL-18 in inflammatory diseases. Nat Rev Rheumatol 20(1):33–47. https://doi.org/10.1038/s41584-023-01053-w
7. Wang Y, Perlman S (2022) COVID-19: inflammatory profile. Annu Rev Med 73:65–80. https://doi.org/10.1146/annurev-med-042220-012417
8. Cheong JG, Ravishankar A, Sharma S, Parkhurst CN, Grassmann SA, Wingert CK et al (2023) Epigenetic memory of coronavirus infection in innate immune cells and their progenitors. Cell 186(18):3882-3902.e3824. https://doi.org/10.1016/j.cell.2023.07.019
9. Mohseni Afshar Z, Barary M, Babazadeh A, Tavakoli Pirzaman A, Hosseinzadeh R, Alijanpour A et al (2023) The role of cytokines and their antagonists in the treatment of COVID-19 patients. Rev Med Virol 33(1):e2372. https://doi.org/10.1002/rmv.2372
10. Vabret N, Britton GJ, Gruber C, Hegde S, Kim J, Kuksin M et al (2020) Immunology of COVID-19: current state of the science. Immunity 52(6):910–941. https://doi.org/10.1016/j.immuni.2020.05.002
11. Dash SP, Gupta S, Sarangi PP (2024) Monocytes and macrophages: Origin, homing, differentiation, and functionality during inflammation. Heliyon 10(8):e29686. https://doi.org/10.1016/j.heliyon.2024.e29686
12. Xie W, Gan J, Zhou X, Tian H, Pan X, Liu W et al (2024) Myocardial infarction accelerates the progression of MASH by triggering immunoinflammatory response and induction of periosti. Cell Metab 36(6):1269-1286.e1269. https://doi.org/10.1016/j.cmet.2024.04.020
13. Kosmider O, Possémé C, Templé M, Corneau A, Carbone F, Duroyon E et al (2024) VEXAS syndrome is characterized by inflammasome activation and monocyte dysregulation. Nat Commun 15(1):910. https://doi.org/10.1038/s41467-024-44811-4
14. Chilunda V, Martinez-Aguado P, Xia LC, Cheney L, Murphy A, Veksler V et al (2021) Transcriptional changes in CD16+ monocytes may contribute to the pathogenesis of COVID-19. Front Immunol 12:665773. https://doi.org/10.3389/fimmu.2021.665773
15. Li H, Liu L, Zhang D, Xu J, Dai H, Tang N et al (2020) SARS-CoV-2 and viral sepsis: observations and hypotheses. Lancet 395(10235):1517–1520. https://doi.org/10.1016/s0140-6736(20)30920-x
16. Zhang Q, Cao X (2021) Epigenetic remodeling in Innate Immunity and Inflammation. Annu Rev Immunol 39:279–311. https://doi.org/10.1146/annurev-immunol-093019-123619
17. Wang R, Lee JH, Kim J, Xiong F, Hasani LA, Shi Y et al (2023) SARS-CoV-2 restructures host chromatin architecture. Nat Microbiol 8(4):679–694. https://doi.org/10.1038/s41564-023-01344-8
18. Chiariello AM, Abraham A, Bianco S, Esposito A, Fontana A, Vercellone F et al (2024) Multiscale modelling of chromatin 4D organization in SARS-CoV-2 infected cells. Nat Commun 15(1):4014. https://doi.org/10.1038/s41467-024-48370-6
19. Giroux NS, Ding S, McClain MT, Burke TW, Petzold E, Chung HA et al (2022) Differential chromatin accessibility in peripheral blood mononuclear cells underlies COVID-19 disease severity prior to seroconversion. Sci Rep 12(1):11714. https://doi.org/10.1038/s41598-022-15668-8
20. Granja JM, Corces MR, Pierce SE, Bagdatli ST, Choudhry H, Chang HY et al (2021) ArchR is a scalable software package for integrative single-cell chromatin accessibility analysis. Nat Genet 53(3):403–411. https://doi.org/10.1038/s41588-021-00790-6
21. Butler A, Hoffman P, Smibert P, Papalexi E, Satija R (2018) Integrating single-cell transcriptomic data across different conditions, technologies, and species. Nat Biotechnol 36(5):411–420. https://doi.org/10.1038/nbt.4096
22. Li Z, Kuppe C, Ziegler S, Cheng M, Kabgani N, Menzel S et al (2021) Chromatin-accessibility estimation from single-cell ATAC-seq data with scOpen. Nat Commun 12(1):6386. https://doi.org/10.1038/s41467-021-26530-2
23. Zhu H, Chen J, Liu K, Gao L, Wu H, Ma L et al (2023) Human PBMC scRNA-seq-based aging clocks reveal ribosome to inflammation balance as a single-cell aging hallmark and super longevity. Sci Adv 9(26):eabq7599. https://doi.org/10.1126/sciadv.abq7599
24. Wang QS, Edahiro R, Namkoong H, Hasegawa T, Shirai Y, Sonehara K et al (2022) The whole blood transcriptional regulation landscape in 465 COVID-19 infected samples from Japan COVID-19 Task Force. Nat Commun 13(1):4830. https://doi.org/10.1038/s41467-022-32276-2
25. Cuomo ASE, Nathan A, Raychaudhuri S, MacArthur DG, Powell JE (2023) Single-cell genomics meets human genetics. Nat Rev Genet 24(8):535–549. https://doi.org/10.1038/s41576-023-00599-5
26. Song T, Yao Y, Papoin J, Sherry B, Diamond B, Gu H et al (2023) Host factor TIMP1 sustains long-lasting myeloid-biased hematopoiesis after severe infection. J Exp Med 220(12). https://doi.org/10.1084/jem.20230018
27. Zhao L, Giannou AD, Xu Y, Shiri AM, Liebold I, Steglich B et al (2021) Efferocytosis fuels malignant pleural effusion through TIMP1. Sci Adv 7(33). https://doi.org/10.1126/sciadv.abd6734
28. Schoeps B, Eckfeld C, Prokopchuk O, Böttcher J, Häußler D, Steiger K et al (2021) TIMP1 triggers neutrophil extracellular trap formation in pancreatic cancer. Cancer Res 81(13):3568–3579. https://doi.org/10.1158/0008-5472.Can-20-4125
29. Mittal P, Roberts CWM (2020) The SWI/SNF complex in cancer - biology, biomarkers and therapy. Nat Rev Clin Oncol 17(7):435–448. https://doi.org/10.1038/s41571-020-0357-3
30. Mashtalir N, Dao HT, Sankar A, Liu H, Corin AJ, Bagert JD et al (2021) Chromatin landscape signals differentially

dictate the activities of mSWI/SNF family complexes. Science 373(6552):306–315. https://doi.org/10.1126/science.abf8705
31. Battistello E, Hixon KA, Comstock DE, Collings CK, Chen X, Rodriguez Hernaez J et al (2023) Stepwise activities of mSWI/SNF family chromatin remodeling complexes direct T cell activation and exhaustion. Mol Cell 83(8):1216-1236.e1212. https://doi.org/10.1016/j.molcel.2023.02.026
32. Liao J, Ho J, Burns M, Dykhuizen EC, Hargreaves DC (2024) Collaboration between distinct SWI/SNF chromatin remodeling complexes directs enhancer selection and activation of macrophage inflammatory genes. Immunity 57(8):1780-1795.e1786. https://doi.org/10.1016/j.immuni.2024.05.008
33. Mittal P, Myers JA, Carter RD, Radko-Juettner S, Malone HA, Rosikiewicz W et al (2024) PHF6 cooperates with SWI/SNF complexes to facilitate transcriptional progression. Nat Commun 15(1):7303. https://doi.org/10.1038/s41467-024-51566-5
34. Malone HA, Roberts CWM (2024) Chromatin remodellers as therapeutic targets. Nat Rev Drug Discov 23(9):661–681. https://doi.org/10.1038/s41573-024-00978-5
35. Sahu RK, Dhakshnamoorthy J, Jain S, Folco HD, Wheeler D, Grewal SIS (2024) Nucleosome remodeler exclusion by histone deacetylation enforces heterochromatic silencing and epigenetic inheritance. Mol Cell 84(17):3175-3191.e3178. https://doi.org/10.1016/j.molcel.2024.07.006